Proceedings of ICMMGH 2026 Symposium: Biomedical Imaging and AI Applications in Neurorehabilitation
DOI: 10.54254/2753-8818/2026.AU30170

Computer-Aided Design of Small Molecules Targeting TNF-α for the Treatment of Crohn's Disease

Wentao He

Scarsdale High School, Scarsdale, USA
wentao.he.2027@gmail.com

Abstract. Crohn's disease (CD) is a chronic inflammatory bowel disease characterized by dysregulated immune responses and intestinal inflammation. Tumor necrosis factor-alpha (TNF-α) is a pro-inflammatory factor that plays an important role in the disease's progression. To treat and manage CD, small molecules have been developed to neutralize TNF-α/TNFR interactions and dampen immune responses as a inexpensive alternative to antibodies. Here, we report a computational pipeline integrating generative molecule design, molecular docking, molecular dynamics (MD) simulations, and an Bayesian optimization framework to optimize small-molecule inhibitors of TNF-α. Starting from a library of ~8,000 compounds derived from the scaffolds of two known TNF-α inhibitors, we implemented the screening pipeline and identified the top candidate WT-7904 with a binding free energy of -58.7 kcal/mol representing a 28.6% improvement relative to Balinatunfib. Structural analyses revealed that hydrophobic contacts, hydrogen bonding, and π-π stacking interactions with tyrosine residues stabilized binding. The ligand binding induced asymmetry of the TNF-α trimer that can potentially impair its receptor binding. Together, these findings identify WT-7904 as a promising lead for the development of small-molecule TNF-α inhibitors and establish a broadly transferable computational framework for accelerating drug discovery in inflammatory diseases such as Crohn's disease.

Keywords: In Silico Design, Virtual Screening, Small Molecule Inhibitors, Molecular Modeling, Machine Learning, TNF-α, Crohn's Disease

1. Introduction

Crohn's disease (CD) is a chronic inflammatory bowel disease (IBD) that can affect any part of the gastrointestinal tract [1]. In North America, the estimated incidence of CD ranges from 96.3 to 318.5 per 100,000 person-years, and its prevalence is steadily increasing worldwide. The CD patients usually exhibit symptoms including abdominal pain, diarrhea, weight loss, and fatigue, which are caused by a dysregulated intestinal immune system and uncontrolled inflammation of the intestines [2]. Although the exact cause of CD remains unclear, current evidence points to the complex interactions between factors like genetic susceptibility, environmental factors, and gut microbiota [3]. These factors collectively drive dysregulated innate and adaptive immune responses, but the mechanisms causing disease's onset and progression are still not fully understood [1,4]. The current treatment for CD only targets the symptoms and reduces inflammation, and no definitive

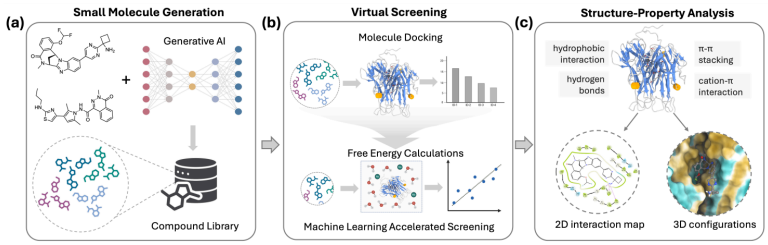
© 2026 The Authors. This is an open access article distributed under the terms of the Creative Commons Attribution License 4.0 (https://creativecommons.org/licenses/by/4.0/).

DOI: 10.54254/2753-8818/2026.AU30170

cure exists as of right now [2,5]. Standard therapy begins with an induction phase using corticosteroids or steroid-like compounds to suppress immune responses, followed by a maintenance phase with lower doses to reduce relapse risk [2]. Long-term management may also target specific immune signaling pathways, including biologic therapies such as monoclonal antibodies against TNF-α, IL-12/23, and integrin $\alpha 4\beta 7$ [2,6].

Since Crohn's disease (CD) is driven by dysregulated immune activity, therapeutic efforts have focused on targeting immune pathways. Tumor necrosis factor-alpha (TNF-α) is one of the most validated targets [7,8]. It is primarily produced by activated macrophages and promotes inflammation by activating a wide range of immune cell types, such as macrophages, T cells, B cells, natural killer (NK) cells, and dendritic cells [9,10]. The binding of TNF-α to its receptor on the cell surface triggers downstream immune signaling cascades that contribute to immune response and thus intestinal epithelial injury and chronic tissue damage [8]. As such, neutralization of TNF-α has become an effective strategy for CD management [11]. For example, monoclonal antibodies have been employed to inhibit their interaction with TNF receptors (TNFRs) on immune cells, which interrupts signaling and attenuates the recruitment and activation of inflammatory cells [12]. This approach has been shown to markedly reduce both inflammation and mucosal damage in patients. To date, the inhibition of cytokine targeting, particularly the TNF-α-TNFR interactions, remains an active field in Crohn's disease research [13].

Despite the effective inhibition of TNF-α, antibodies or engineered biologics are limited due to their high cost and difficulty of delivery [14]. Small molecules are potential alternatives for disrupting TNF-receptor interactions [15]. However, research has demonstrated that existing small molecules targeting TNF-α require further optimization and development to achieve higher efficacy [16]. The chemical space of potential small molecules is vast, making drug design and screening a resource-intensive and laborious task [17]. To address the challenge, virtual screening that combines physics-modeling [18] and machine learning techniques [19] has been widely employed to accelerate the discovery of drug molecules. Molecular docking has been widely used to rapidly identify hit compounds within large chemical libraries [20], which is usually followed by free energy calculation from molecular dynamics (MD) simulations [21] to offer greater accuracy for refining and optimizing candidate molecules [22]. More recently, artificial intelligence (AI) and machine learning algorithms have been integrated into virtual screening processes for the generation and prioritization of novel small molecules [23-26]. The interplay of molecular modeling and machine learning offers an effective strategy to traverse large chemical libraries and accelerate drug discovery.



Scheme 1. Schematic illustration of the workflow for designing and screening novel compounds for TNF-α inhibition. (a) Generative AI-enabled small molecule library construction using REINVENT based on existing inhibitors. (b) High throughput virtual screening using molecular docking, free-energy calculations, and machine learning to prioritize candidate binders for evaluations. (c) Proposal of the top novel drug candidates and structure-property analysis of relaxed complexes using 2D interaction maps and 3D structural visualization to reveal binding molecular forces

DOI: 10.54254/2753-8818/2026.AU30170

Herein, we established a high-throughput virtual screening (HTVS) pipeline that integrates generative AI-enabled compound library generation, molecular docking, free energy calculations and active learning to identify novel small molecule inhibitors of TNF-α (**Scheme 1**). A library comprising approximately 8000 compounds was generated using the REINVENT [27] model by modifying and decorating two known small molecule inhibitors: Balinatunfib [28] and TIM1c [29] (**Scheme 1a**). All compounds were then docked into the binding pocket of a TNF-α trimer, and a subset of the molecules with the most favorable docking scores was selected for further evaluation (**Scheme 1b**). Subsequently, we coupled active learning and free energy calculation from MD simulations to efficiently traverse this chemical space. During the process, a surrogate model was trained on calculated free energies to perform predictions across the library and to iteratively guide the selection of new candidates for evaluation (**Scheme 1b**). This iterative workflow enabled the identification of top candidates without exhaustive evaluation of the entire chemical library. Final structural analyses of protein-ligand complexes were conducted to extract design principles (**Scheme 1c**). From this workflow, we identified ten compounds with binding free energies lower than that of the reference drug Balinatunfib. Among these, WT-7904 emerged as the top candidate with a free energy of -58.7 kcal/mol, bettering Balinatunfib by 28.6%. Structural analysis further revealed that hydrophobic contacts, polar interactions, and multiple π-π stacking interactions with tyrosine residues in the binding pocket were the primary forces stabilizing ligand binding. Notably, WT-7904 also distorted the symmetric trimer structure of TNF-α and further supported its ability to inhibit the binding affinity of TNF-α to its receptor. Overall, the computational pipeline greatly accelerated the discovery of novel inhibitors of TNF-α, revealed design principles for these molecules, and furnished a transferable computational framework for designing small molecules with desirable structural or functional properties.

2. Computational methods

2.1. Compound library generation

As the basis of our compound library, two previously reported TNF-α inhibitors, Balinatunfib [28] and TIM1c [29], were chosen for the library generation. The molecules were employed as the template molecules in the REINVENT model [27], which is a generative deep learning software for *de novo* design. REINVENT uses recurrent neural networks [30] and transformer architectures [31] to generate chemical structures in SMILES format while considering factors such as binding potential and structural similarity to the base molecule. To ensure synthetic feasibility of AI-generated molecules, we avoided random atom insertions or arbitrary permutations into the core scaffolds of the reference molecules and introduced modifications only to the functional groups. With the REINVENT platform, we generated a chemical library of 7947 compounds, including the original reference molecules, with overall medium to high structural similarity measured by the model. The library is then used as the basis for subsequent stages of molecular docking and MD simulations (**Figure S1**).

2.2. Molecular docking

After the library construction, we first employed molecular docking as the first screening filter to narrow down the chemical space. We first obtained the three-dimensional structure of TNF-alpha trimer (PDB ID: 6OOY) from the RCSB Protein Data Bank (PDB) and then employed UCSF Chimera's Modeller [32] tool to reconstruct the truncated regions of the protein. After processing,

DOI: 10.54254/2753-8818/2026.AU30170

we prepared the protein grid for docking by constructing a box with a length of 3 nm centered around 6OOY's binding pocket. AutoDock Vina [33] was used for molecular docking and to obtain the binding pose of the compounds in the generated library. To account for the flexibility of the binding pocket during protein-ligand binding, we treated residues Tyr59, Tyr119, and Tyr151 of each chain as flexible [34]. Subsequently, each of our 7947 compounds was docked into the box with an exhaustiveness of 32. For each receptor-ligand pair, we only kept the best pose. The docked complex was finally assembled by combining the receptor and the best pose of the ligand.

2.3. Molecular dynamics simulations and free energy calculation

Following docking, we performed MD simulations to more accurately evaluate the stability of the protein-ligand binding complex and to calculate the binding free energy. The simulations were implemented using GROMACS 2024.4 software [35,36]. The AMBERff99SB force field [37] was used for the protein structure. The topology of the small molecules was prepared using Acpype with the GAFF2 force field [38-40]. Then, the protein-ligand complex was placed at the center of a cube-shaped box with periodic boundaries to replicate an infinite system. The box was solvated with TIP3P [41] water molecules, and the charge of the system was balanced by sodium and chloride ions to reach a salt concentration of 0.15 M.

In all simulations, energy minimization was carried out using the steepest descent algorithm to eliminate forces larger than 1000 $kJ/mol \cdot nm^2$. For all simulations, the temperature was set to 300 K by velocity-rescale [42] thermostat with a time constant of 2 ps. Following energy minimization, the NVT simulation was performed for 100 ps. Finally, we ran the NPT simulation for 5 ns at 1 bar by c-rescale [43] barostat with a time constant of 12 ps and a compressibility of 3.0×10^{-4}/bar. The time step was set to 2 fs for both equilibration and production run, and Newton's equations of motion were integrated by the leap-frog algorithm [44]. The long-range electrostatics were treated with the particle mesh Ewald (PME) algorithm [45]. A cut-off distance of 1.0 nm was used for van der Waals and short-range electrostatic interactions. The analyses of the simulation trajectories were performed using MDAnalysis [46]. ChimeraX [47] was used to visualize the simulation snapshots, and plots were generated using matplotlib [48].

Once we obtained the simulation frames, the binding scores were computed using the MM/PBSA (or MM/GBSA) theory [49] with gmx_MMPBSA [50]. A multiple-frame scheme was used to obtain a more reliable estimate of the ΔG values and the associated uncertainty. The calculation was performed for the final 2.5 ns simulation comprising 50 frames of trajectories. In addition, we also extracted root mean square deviation (RMSD) profiles of the ligands in the protein pocket using MDAnalysis [46] to infer the conformational stability.

2.4. Gaussian process regression and bayesian optimization

Given the ΔG values we obtained for a subset of the library, we then aim to utilize machine learning surrogate models to predict the ΔG's of the remaining candidates from the narrowed design space for next-round simulations. We employed a GPR model [51], which is constructed by a kernel function that represents the similarity of each molecule pair. The molecule was represented by Morgan fingerprints with a radius of 2 and a bit length of 2048 using RDKit [52]. Molecular similarity was quantified using the Tanimoto kernel function, where the Jaccard similarity between pairs of bit vectors was used to build the covariance matrix [53].

The active learning process began with an initial set of 94 compounds selected from the design library for MD simulations. The selection of the seed compound was conducted by uniform

DOI: 10.54254/2753-8818/2026.AU30170

sampling in a reduced feature space obtained by applying PCA to the molecular fingerprints to ensure a broad and uniform coverage of the chemical space. MD simulations were then implemented for these compounds, and the resulting free energy values were extracted and used as training data for the GPR model.

Subsequent rounds of compound selection were guided by Bayesian optimization (BO) [54]. In this framework, the expensive objective function (ΔG from MD simulations) is modeled by a surrogate model (GPR), which is iteratively updated as new data become available. At each round, an acquisition function is employed to propose new candidates that are likely to improve the objective function. The newly evaluated data are then incorporated into the training set to refine the GPR model and guide the next iteration. This iterative loop allows an efficient navigation of the chemical space while minimizing the number of costly MD simulations.

The candidate selection was guided by the upper confidence bound (UCB) acquisition function [55] that balances exploration of uncertain regions with exploitation of regions predicted to yield favorable free energies. It mainly proposes compounds that are most likely to be better performing than the current ones for evaluation. The upper confidence bound acquisition has a form

$$\mathrm{UCB} = \mu(\mathrm{x}) + \beta\sigma(\mathrm{x}) \tag{1}$$

where $\mu(x)$ and $\sigma(x)$ denote the prediction mean and the standard deviation of the surrogate model at the candidate x. The parameter β is a tunable parameter in the acquisition function that balances exploration and exploitation of the chemical space. Larger β values increase the weight of predictive uncertainty and propose compounds in unexplored regions where evaluated samples are scarce (exploration). Smaller β values put more emphasis on predicted values to prioritize compounds that are expected to offer favorable ΔG values (exploitation). In our implementation, we set $\beta = 0.1$ for the first five rounds to balance exploration and exploitation. From round 5 onward, β was reduced to 0 to enforce pure exploitation and prioritize compounds with the lowest predicted free energies (i.e., highest binding affinity). In each round, batches of 10 candidates were proposed, evaluated, and incorporated into the training set to refine the model. The active learning process was terminated at round 12, when no further improvement in ΔG values was observed. All active learning steps were carried out using the BoTorch [56] library.

3. Results

3.1. Binding mode of TNF-α inhibitors and library construction

Prior to screening the chemical library, we first examined the structure of a TNF-α protein and the binding modes of the known inhibitors, including Balinatunfib and TIM1c. TNF-α is a pro-inflammatory cytokine that forms a compact bell-shaped trimer (**Figure 1a**). It is composed of three identical monomers that associate around a 3-fold axis, with each monomer being an elongated and antiparallelβ-pleated sheet sandwich [57]. Given the trimer nature of TNF-α, small molecules such as Balinatunfib can bind to the allosteric pocket in the TNF-α trimer (**Figure 1b**). Upon binding, Balinatunfib induces a conformational shift that converts TNF-α into an asymmetric and non-signaling structure [58]. The distortion then weakens the binding of TNF-α to TNFR and subsequently shuts down the inflammatory signaling cascade [28].

The binding pocket of TNF-α is predominantly hydrophobic [59] (**Figure 1b**). The binding complex between Balinatunfib and TNF-α is largely driven by hydrophobic interactions

DOI: 10.54254/2753-8818/2026.AU30170

supplemented with π-π stacking with the tyrosine residue of the three subunits (**Figure 1c**). In addition to these interactions, hydrogen bonds and cation-π interactions further enhance the binding affinity. Similarly, compared to Balinatunfib, TIM1c also demonstrates mainly hydrophobic and π-π stacking interactions [29] (**Figure 1c**).

To discover molecules with potentially improved binding affinity for TNF-α, we constructed a chemical library using Balinatunfib and TIM1c as starting scaffolds. Using the generative deep learning model REINVENT [27], we generated a chemical library of 7947 compounds. Since both Balinatunfib and TIM1c have shown promising efficacy in disrupting TNF-α signaling, we designed our compound library to maintain a relatively high degree of similarity to these scaffolds (**Figure 1d**). This strategy ensured that newly generated molecules may preserve the essential binding motifs and physicochemical properties responsible for their activity, such as hydrophobic contacts, π-π stacking interactions with tyrosine residues, and stabilizing hydrogen bonds within the allosteric pocket. At the same time, the generative design process introduced structural variations, such as alternative ring substitutions, heteroatom incorporation, or side-chain modifications, that expanded chemical diversity. In doing so, our virtual screening efforts were biased toward compounds with both a strong likelihood of retaining efficacy and the potential to exhibit improved binding affinity or novel interaction profiles compared to the parent inhibitors.

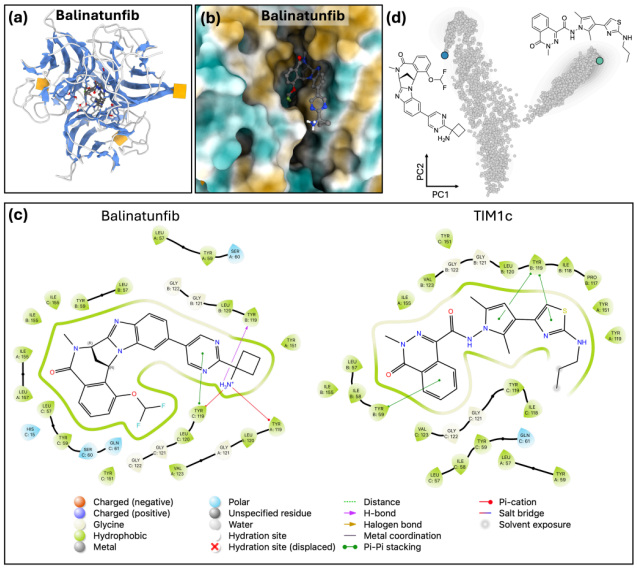


Figure 1. Docking and structural characterization of TNF-α inhibitors. (a) Overall binding pose of the docked Balinatunfib within the TNF-α trimer after MD relaxation. (b) Surface representation of the binding pocket highlighting hydrophobic (yellow) and polar regions around the ligand Balinatunfib. Chain A is omitted for clarity. (c) 2D interaction diagram showing key hydrogen bonds, hydrophobic contacts, cation-π, and π-π stacking interactions of Balinatunfib and TIM1c in the binding pocket. (d) A PCA plot of the distribution of the designed chemical library consisting of 7947 molecules. The initial seeding drug molecules are highlighted. Molecular renderings in (a) and (b) were generated by ChimeraX REF _Ref28595 \r \h [47], and the interaction diagrams in (c) were created by Maestro Viewer

DOI: 10.54254/2753-8818/2026.AU30170

3.2. Prioritization of compounds by molecular docking

Out of our initial 7949 compounds, we were able to successfully dock 7857 of those compounds. The remaining 92 compounds failed to dock in the binding pocket either because their large molecular size induced large molecular forces in the binding pocket or because their compound structure was invalid. The effectiveness of each compound was measured and ranked by its evaluated docking score, with lower scores indicating higher binding strength to TNF-α. The binding scores are shown in **Figure 2a**. To prioritize candidates, we applied Balinatunfib's docking score of -11.26 kcal/mol as a threshold to focus subsequent analyses on compounds with equal or greater predicted affinity (**Figure 2a**). This led to a narrowed chemical space comprising 1361 molecules. This reduction in chemical space enabled more rigorous downstream simulations on a refined set of promising molecules.

Among the docked compounds, WT-4148 emerged as the top candidate with the lowest docking score. It is structurally derived from Balinatunfib and preserves its core scaffold while incorporating additional polar regions. Its binding mode involved hydrophobic contacts and multiple π-π stacking interactions with Tyr59 and Tyr119 in the binding pocket (**Figure 2b**). These features resemble the key interaction patterns observed for Balinatunfib and TIM1c and confirm that the generative design strategy effectively conserved critical binding interactions. From this narrowed subset, we proceeded with molecular dynamics simulations and involved an active learning workflow to refine the ranking of candidate compounds and identify the most promising inhibitors.

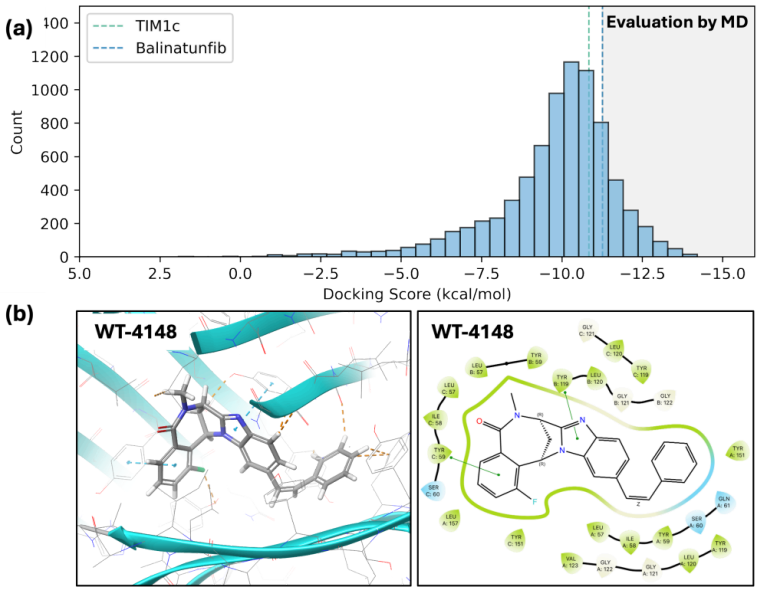


Figure 2. Prioritization of compounds by brute force docking. (a) The distribution of the docking scores of the 7949 compounds in the design library. The dashed lines indicate the docking scores of the existing drugs TIM1c and Balinatunfib, and the shaded area denotes the compounds that are selected from docking for the subsequent active learning pipeline screening in which MD simulations were coupled with machine learning to further optimize the ranking of the candidates. (b) The 3D (left) and 2D (right) interaction schemes of the best molecule identified by docking (WT-4148). The interaction diagrams were created using Maestro Viewer

DOI: 10.54254/2753-8818/2026.AU30170

3.3. Identification of top candidates by an active learning pipeline

With the reduced design space, we implemented an active learn (AL) pipeline that combines MD simulations with machine learning to effectively select the most promising molecules to the TNF-α protein. The active learning pipeline started with an initialization of 85 compounds for MD simulations and free energy calculations. In each subsequent round, the GPR model was trained using the accumulated simulation data and then employed to propose ten new candidates predicted to balance exploration of chemical diversity with exploitation of high-affinity regions of the design space for another round of MD evaluation.

In total, we performed 12 rounds of active learning using the upper bound confidence acquisition function. Over the course of AL, the pipeline demonstrated a progressive improvement in the proposed compounds. The most potent molecule in the seeding round has a ΔG of -47.7 kcal/mol (**Figure 3a**). As the process progressed, the median and the cumulative best binding free energies displayed a downward trend, indicating that the active learning strategy progressively proposed candidates with improved predicted binding affinity. By round 8, the campaign identified a candidate with a ΔG of -58.74 kcal/mol, showing a significant improvement over the initial pool. The cumulative best and the top 10 compounds stabilize in later rounds, suggesting that the pipeline successfully converged on high-affinity candidates by 12 rounds. Overall, we performed MD simulations on 196 compounds out of the 1361 that passed the docking score threshold. Through the AL pipeline, we were able to significantly identify top candidates with high predicted efficacy while simulating less than 20% of the initial candidates, which greatly increased the screening efficiency.

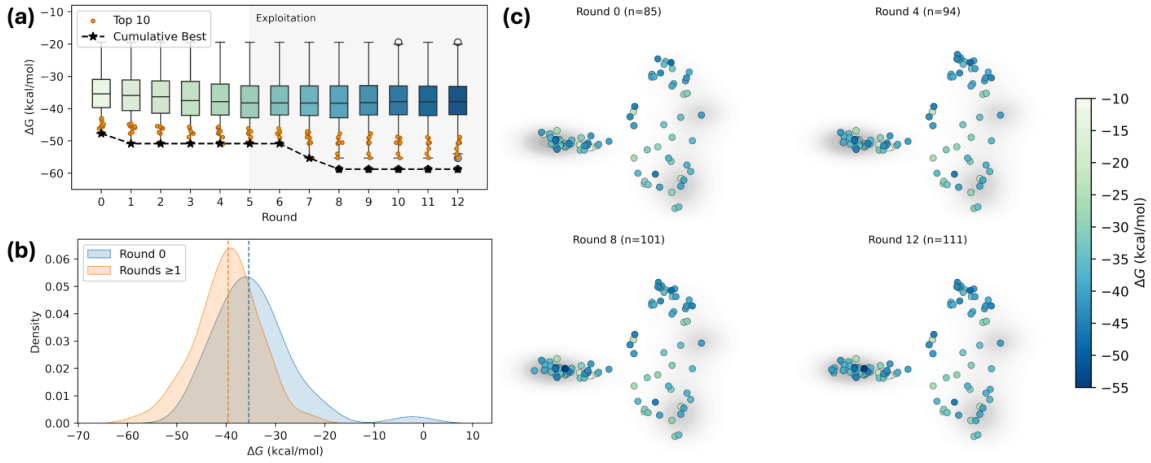


Figure 3. The active learning process in the narrowed design space by molecular docking. (a) The box plot showing the distribution of cumulative ΔG values in each round. The orange dots represent the cumulative top 10 molecules, and the black line denotes the cumulative top molecule up to each round. (b) The density plot of the ΔG values in round 0 (blue) and those in round 1-12 (orange). The dashed lines show the median ΔG in each group. (c) The PCA plot showing the progressive labeling of putative molecules in round 0, 4, 8 and 12. The gray shaded area shows the density of molecules and the colors represent the ΔG values

Likewise, the distribution of ΔG for all subsequent rounds (rounds ≥ 1) is better than the distribution of the initial round (round 0) (**Figure 3b**). The median of the initial distribution is centered at -35 kcal/mol. By comparison, the median of subsequent rounds shifted the distribution left, to a median ΔG of approximately -39 kcal/mol. The leftward shift towards a lower binding

DOI: 10.54254/2753-8818/2026.AU30170

affinity demonstrates the efficient prioritization of the potent compounds by the machine learning model in the screening process.

In **Figure 3c**, we show the distribution of sampled molecules across some representative rounds to illustrate the progressive enrichment of top compounds. In the initial round, molecules were broadly selected from all major regions of the chemical space. As the campaign progressed, the acquisition function increasingly concentrated on sampling the neighborhoods associated with high binding affinities. This observation is in alignment with the continuous improvement of the top candidates from round 6 to round 8 in **Figure 3a.**Through this process, the AL pipeline was able to effectively identify potent TNF-α inhibitors from the large chemical library.

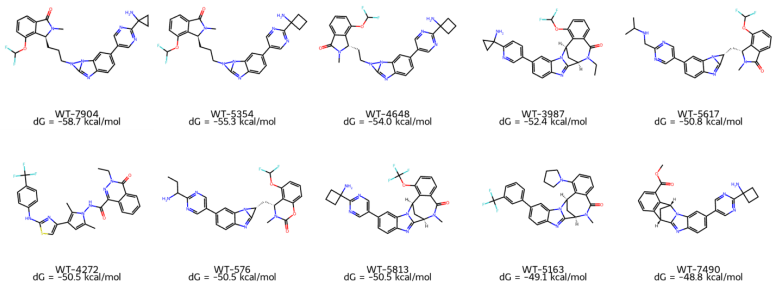


Figure 4. The identified top molecules from the computational screening. The molecule WT-7904 emerges as the top candidate ranked by binding free energy. The structures were visualized by RDKit

Once we converged on the top 10 candidates, we terminated the active learning process and subjected these molecules to detailed analysis. Using the binding free energy (ΔG) as a proxy for affinity, we identified the 10 molecules with the lowest ΔG values (**Figure 4**). Free energy reflects the thermodynamic difference between the ligand-bound and unbound states, thereby quantifying the stabilization of TNF-α upon ligand binding. All top candidates remained stably bound in the TNF-α pocket, showing average heavy-atom RMSD values below 3.0 Å (mostly under 2.0 Å) consistent with their favorable binding energies (**Figure 5**). Among these, WT-7904 emerged as the top candidate with a ΔG of -58.7 kcal/mol, which is substantially lower than that of Balinatunfib (-45.65 kcal/mol). This represents a ~28.6% improvement in predicted binding affinity. These findings underscore their ability to bind to TNF-α function and support their potentially improved efficacy in further experimental validation.

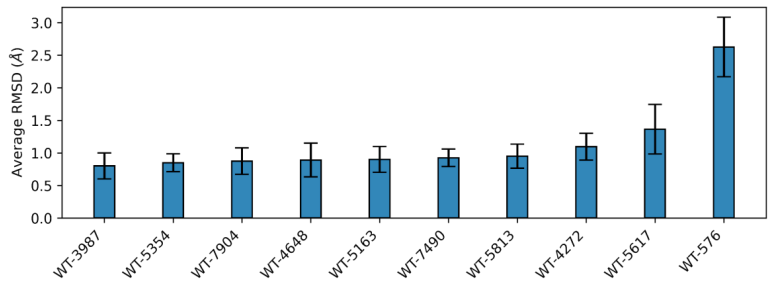


Figure 5. Average RMSD values of the proposed molecules in the binding pocket from the MD simulations. The low values indicate the stable conformations of all ligands in the binding pocket

DOI: 10.54254/2753-8818/2026.AU30170

3.4. Structure-property relationship of top candidates

Having identified the top candidates from the design library, we then sought to understand the molecular interactions that contribute to the stable binding of these candidates. In **Figure 6**, we show the interaction diagrams of the top candidate WT-7904. It exhibits a dominant network of hydrophobic contacts with residues that define the TNF-α binding pocket, including leucine, valine, isoleucine and multiple tyrosine residues. These interactions stabilize the ligand within the largely hydrophobic cleft, while additional π-π stacking interactions with aromatic side chains, particularly Tyr-59 and Tyr-373, further anchor the compound. In addition, the compound exhibits a network of hydrogen bonds between the protonated amine group with the protein side chains or backbone. The combined effect of aromatic stacking and hydrogen bonding strengthens ligand-protein contacts and leads to greater overall binding affinity and correspondingly lower binding free energy compared with the original base structures.

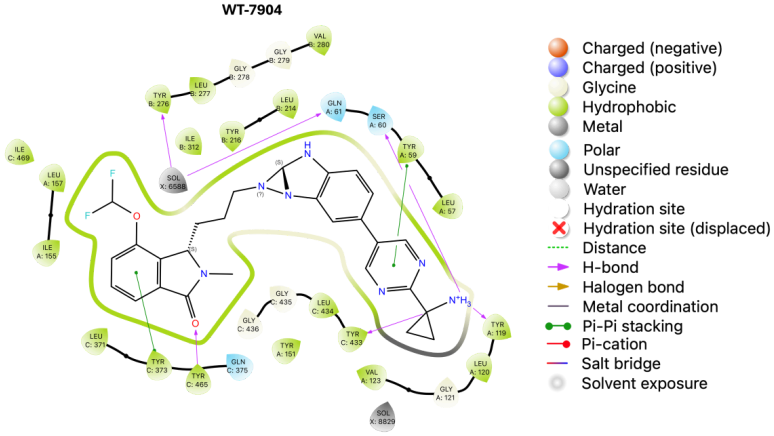


Figure 6. 2D ligand-protein interaction diagrams of the top-scoring compound, WT-7904. The diagram shows the ligand in complex with the binding pocket residues, highlighting hydrogen bonds, hydrophobic contacts, and π–π stacking interactions. The diagram was generated by Maestro Viewer

Building on the molecular interaction analysis, where WT-7904 demonstrated extensive molecular interactions with protein pockets, we next examined the effect of ligand binding on the overall TNF-α trimer structure. These local interactions not only account for the strong binding affinity of WT-7904 but also translate into broader conformational consequences for the protein. As shown in **Figure 7**, the unbound TNF-α exhibits a symmetric trimeric organization (**Figure 7a**). This geometry is required for proper binding with TNF-α receptors. In contrast, when WT-7904 is bound in the protein pocket, the trimer shows a distorted and asymmetric structure where chain A is shifted downwards as indicated by the red arrows (**Figure 7b**). This asymmetry destabilizes one of the receptor-binding interfaces and thus reduces receptor binding capacity. Such ligand-induced disruption prevents efficient receptor clustering on the cell surface and impairs TNF-α-mediated signaling. Together, the combination of favorable molecular interactions and the ligand-driven distortion of the trimer confirms WT-7904's strong potential as a novel TNF-α inhibitor.

DOI: 10.54254/2753-8818/2026.AU30170

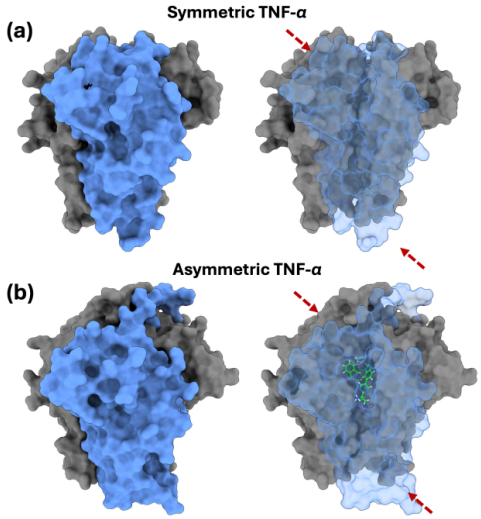


Figure 7. The demonstration of symmetry breaking of the TNF-α trimer by the binding of ligand WT-7904. (a) A symmetric structure of TNF-α in a functioning form (PDB ID: 6RMJ). (b) Simulated asymmetric TNF-α trimer caused by binding of the small-molecule ligand WT-7904 (green) within the inter-subunit pocket. In both structures, chain A is highlighted in blue for reference. Chains B and C are shown in gray. Red dashed arrows indicate the regions of structural deviation between symmetric and asymmetric states. The representations were rendered using ChimeraX REF _Ref28595 \r \h [47]

4. Conclusion and discussion

In this study, we established a virtual screening pipeline to identify novel small-molecule inhibitors of TNF-α with therapeutic potential for Crohn's disease. Our workflow integrated generative AI, molecular docking, MD simulations, and an active learning framework based on Gaussian process regression and Bayesian optimization. Starting from a library of 7,947 compounds derived from the scaffolds of two known TNF-α inhibitors, Balinatunfib and TIM1c, we applied the screening pipeline and identified WT-7904 as the most promising candidate with a binding free energy of -58.7 kcal/mol, representing a ~28.6% improvement over Balinatunfib (-45.65 kcal/mol). Structural and interaction analyses revealed that the enhanced affinity of WT-7904 and other top candidates arises from a combination of hydrophobic contacts, π-π stacking interactions with aromatic residues, and a network of hydrogen bonds. Importantly, these interactions induce conformational asymmetry in the TNF-α trimer, which may potentially disrupt the receptor-binding interfaces and thereby impair TNFR engagement. Such destabilization of TNF-α highlights WT-7904's potential as a potent inhibitor and a promising lead for the development of new therapies for Crohn's disease.

Despite the encouraging performance of the identified small-molecule candidates, certain aspects of the virtual screening pipeline can benefit from further improvement. First, expanding the chemical library to include greater structural diversity and more scaffolds could further enrich the exploration of chemical space and uncover novel lead compounds [60,61]. Second, the free energy calculations used to prioritize candidates could be strengthened by extending simulation time scales or by employing advanced approaches such as enhanced sampling [62] or alchemical free energy methods [63], to improve the accuracy and reliability of binding free energy estimates. Finally, experimental validation of the top-ranked candidates would be the top priority following this work, such as*in vitro* binding assays, or cellular studie.

DOI: 10.54254/2753-8818/2026.AU30170

Overall, we developed a computational pipeline integrating physics-based modeling and machine learning to greatly accelerate the design of small molecule inhibitors of TNF-α and proposed a number of novel candidates for experimental testing for Crohn's disease. Furthermore, beyond the present focus on TNF-α inhibition, the pipeline developed in this work is broadly transferable to other small-molecule discovery endeavors, providing a generalizable strategy for the design, evaluation, and optimization of small-molecule therapeutics.

References

[1] Torres, J.; Mehandru, S.; Colombel, J.-F.; Peyrin-Biroulet, L. Crohn's Disease. The Lancet 2017, 389 (10080), 1741–1755. https: //doi.org/10.1016/S0140-6736(16)31711-1.

[2] Cushing, K.; Higgins, P. D. R. Management of Crohn Disease: A Review. JAMA 2021, 325 (1), 69. https: //doi.org/10.1001/jama.2020.18936.

[3] Akiyama, S.; Nishijima, S.; Kojima, Y.; Kimura, M.; Ohsugi, M.; Ueki, K.; Mizokami, M.; Hattori, M.; Tsuchiya, K.; Uemura, N.; Kawai, T.; Bork, P.; Nagata, N. Multi-Biome Analysis Identifies Distinct Gut Microbial Signatures and Their Crosstalk in Ulcerative Colitis and Crohn's Disease. Nat Commun 2024, 15 (1), 10291. https: //doi.org/10.1038/s41467-024-54797-8.

[4] Jaeger, N.; Gamini, R.; Cella, M.; Schettini, J. L.; Bugatti, M.; Zhao, S.; Rosadini, C. V.; Esaulova, E.; Di Luccia, B.; Kinnett, B.; Vermi, W.; Artyomov, M. N.; Wynn, T. A.; Xavier, R. J.; Jelinsky, S. A.; Colonna, M. Single-Cell Analyses of Crohn's Disease Tissues Reveal Intestinal Intraepithelial T Cells Heterogeneity and Altered Subset Distributions. Nat Commun 2021, 12 (1), 1921. https: //doi.org/10.1038/s41467-021-22164-6.

[5] Vieujean, S.; Jairath, V.; Peyrin-Biroulet, L.; Dubinsky, M.; Iacucci, M.; Magro, F.; Danese, S. Understanding the Therapeutic Toolkit for Inflammatory Bowel Disease. Nat Rev Gastroenterol Hepatol 2025, 22 (6), 371–394. https: //doi.org/10.1038/s41575-024-01035-7.

[6] Thomas, T.; Friedrich, M.; Rich-Griffin, C.; Pohin, M.; Agarwal, D.; Pakpoor, J.; Lee, C.; Tandon, R.; Rendek, A.; Aschenbrenner, D.; Jainarayanan, A.; Voda, A.; Siu, J. H. Y.; Sanches-Peres, R.; Nee, E.; Sathananthan, D.; Kotliar, D.; Todd, P.; Kiourlappou, M.; Gartner, L.; Ilott, N.; Issa, F.; Hester, J.; Turner, J.; Nayar, S.; Mackerodt, J.; Zhang, F.; Jonsson, A.; Brenner, M.; Raychaudhuri, S.; Kulicke, R.; Ramsdell, D.; Stransky, N.; Pagliarini, R.; Bielecki, P.; Spies, N.; Marsden, B.; Taylor, S.; Wagner, A.; Klenerman, P.; Walsh, A.; Coles, M.; Jostins-Dean, L.; Powrie, F. M.; Filer, A.; Travis, S.; Uhlig, H. H.; Dendrou, C. A.; Buckley, C. D. A Longitudinal Single-Cell Atlas of Anti-Tumour Necrosis Factor Treatment in Inflammatory Bowel Disease. Nat Immunol 2024, 25 (11), 2152–2165. https: //doi.org/10.1038/s41590-024-01994-8.

[7] Van Loo, G.; Bertrand, M. J. M. Death by TNF: A Road to Inflammation. Nat Rev Immunol 2023, 23 (5), 289–303. https: //doi.org/10.1038/s41577-022-00792-3.

[8] Palucka, A. K.; Blanck, J.-P.; Bennett, L.; Pascual, V.; Banchereau, J. Cross-Regulation of TNF and IFN-α in Autoimmune Diseases. Proc. Natl. Acad. Sci. U.S.A. 2005, 102 (9), 3372–3377. https: //doi.org/10.1073/pnas.0408506102.

[9] Alam, M. S.; Otsuka, S.; Wong, N.; Abbasi, A.; Gaida, M. M.; Fan, Y.; Meerzaman, D.; Ashwell, J. D. TNF Plays a Crucial Role in Inflammation by Signaling via T Cell TNFR2. Proc. Natl. Acad. Sci. U.S.A. 2021, 118 (50), e2109972118. https: //doi.org/10.1073/pnas.2109972118.

[10] Adjuto-Saccone, M.; Soubeyran, P.; Garcia, J.; Audebert, S.; Camoin, L.; Rubis, M.; Roques, J.; Binétruy, B.; Iovanna, J. L.; Tournaire, R. TNF-α Induces Endothelial–Mesenchymal Transition Promoting Stromal Development of Pancreatic Adenocarcinoma. Cell Death Dis 2021, 12 (7), 649. https: //doi.org/10.1038/s41419-021-03920-4.

[11] Grijalva, C. G.; Chen, L.; Delzell, E.; Baddley, J. W.; Beukelman, T.; Winthrop, K. L.; Griffin, M. R.; Herrinton, L. J.; Liu, L.; Ouellet-Hellstrom, R.; Patkar, N. M.; Solomon, D. H.; Lewis, J. D.; Xie, F.; Saag, K. G.; Curtis, J. R. Initiation of Tumor Necrosis Factor-α Antagonists and the Risk of Hospitalization for Infection in Patients With Autoimmune Diseases. JAMA 2011, 306 (21). https: //doi.org/10.1001/jama.2011.1692.

[12] Kumar, M.; Murugesan, S.; Ibrahim, N.; Elawad, M.; Al Khodor, S. Predictive Biomarkers for Anti-TNF Alpha Therapy in IBD Patients. J Transl Med 2024, 22 (1), 284. https: //doi.org/10.1186/s12967-024-05058-1.

[13] Neurath, M. F. Targeting Cytokines in Inflammatory Bowel Disease. Sci. Transl. Med. 2022, 14 (675), eabq4473. https: //doi.org/10.1126/scitranslmed.abq4473.

[14] Chames, P.; Van Regenmortel, M.; Weiss, E.; Baty, D. Therapeutic Antibodies: Successes, Limitations and Hopes for the Future. British J Pharmacology 2009, 157 (2), 220–233. https: //doi.org/10.1111/j.1476-5381.2009.00190.x.

DOI: 10.54254/2753-8818/2026.AU30170

[15] O'Connell, J.; Porter, J.; Kroeplien, B.; Norman, T.; Rapecki, S.; Davis, R.; McMillan, D.; Arakaki, T.; Burgin, A.; Fox Iii, D.; Ceska, T.; Lecomte, F.; Maloney, A.; Vugler, A.; Carrington, B.; Cossins, B. P.; Bourne, T.; Lawson, A. Small Molecules That Inhibit TNF Signalling by Stabilising an Asymmetric Form of the Trimer. Nat Commun 2019, 10 (1), 5795. https: //doi.org/10.1038/s41467-019-13616-1.

[16] Melagraki, G.; Ntougkos, E.; Rinotas, V.; Papaneophytou, C.; Leonis, G.; Mavromoustakos, T.; Kontopidis, G.; Douni, E.; Afantitis, A.; Kollias, G. Cheminformatics-Aided Discovery of Small-Molecule Protein-Protein Interaction (PPI) Dual Inhibitors of Tumor Necrosis Factor (TNF) and Receptor Activator of NF-κB Ligand (RANKL). PLoS Comput Biol 2017, 13 (4), e1005372. https: //doi.org/10.1371/journal.pcbi.1005372.

[17] Reymond, J.-L. The Chemical Space Project. Acc. Chem. Res. 2015, 48 (3), 722–730. https: //doi.org/10.1021/ar500432k.

[18] Muegge, I.; Hu, Y. Recent Advances in Alchemical Binding Free Energy Calculations for Drug Discovery. ACS Med. Chem. Lett. 2023, 14 (3), 244–250. https: //doi.org/10.1021/acsmedchemlett.2c00541.

[19] Lindley, S. E.; Lu, Y.; Shukla, D. The Experimentalist's Guide to Machine Learning for Small Molecule Design. ACS Appl. Bio Mater. 2024, 7 (2), 657–684. https: //doi.org/10.1021/acsabm.3c00054.

[20] Gentile, F.; Agrawal, V.; Hsing, M.; Ton, A.-T.; Ban, F.; Norinder, U.; Gleave, M. E.; Cherkasov, A. Deep Docking: A Deep Learning Platform for Augmentation of Structure Based Drug Discovery. ACS Cent. Sci. 2020, 6 (6), 939–949. https: //doi.org/10.1021/acscentsci.0c00229.

[21] Knight, J. L.; Clark, A. J.; Wang, J.; Placzek, A.; Bos, P. H.; Bhat, S.; Bell, J. A.; Silvergleid, S.; Yin, W.; Gray, F.; Sun, S.; Akinsanya, K.; Abel, R.; Gerasyuto, A. I. Harnessing Free Energy Calculations for Kinome-Wide Selectivity in Drug Discovery Campaigns with a Wee1 Case Study. Nat Commun 2025, 16 (1), 7962. https: //doi.org/10.1038/s41467-025-62722-w.

[22] Sharma, H.; Sharma, P.; Urquiza, U.; Chastain, L. R.; Ihnat, M. A. Exploration of a Large Virtual Chemical Space: Identification of Potent Inhibitors of Lactate Dehydrogenase-A against Pancreatic Cancer. J. Chem. Inf. Model. 2023, 63 (3), 1028–1043. https: //doi.org/10.1021/acs.jcim.2c01544.

[23] Alakhdar, A.; Poczos, B.; Washburn, N. Diffusion Models in De Novo Drug Design. J. Chem. Inf. Model. 2024, 64 (19), 7238–7256. https: //doi.org/10.1021/acs.jcim.4c01107.

[24] Gangwal, A.; Lavecchia, A. Unleashing the Power of Generative AI in Drug Discovery. Drug Discovery Today 2024, 29 (6), 103992. https: //doi.org/10.1016/j.drudis.2024.103992.

[25] Wang, L.; Zhou, Z.; Yang, X.; Shi, S.; Zeng, X.; Cao, D. The Present State and Challenges of Active Learning in Drug Discovery. Drug Discovery Today 2024, 29 (6), 103985. https: //doi.org/10.1016/j.drudis.2024.103985.

[26] Gusev, F.; Gutkin, E.; Kurnikova, M. G.; Isayev, O. Active Learning Guided Drug Design Lead Optimization Based on Relative Binding Free Energy Modeling. J. Chem. Inf. Model. 2023, 63 (2), 583–594. https: //doi.org/10.1021/acs.jcim.2c01052.

[27] Loeffler, H. H.; He, J.; Tibo, A.; Janet, J. P.; Voronov, A.; Mervin, L. H.; Engkvist, O. Reinvent 4: Modern AI–Driven Generative Molecule Design. J Cheminform 2024, 16 (1), 20. https: //doi.org/10.1186/s13321-024-00812-5.

[28] Dömling, A.; Holak, T. A. Balinatunfib: A Clinical Oral Small Molecule TNFα Inhibitor. ChemMedChem 2025, 20 (14), e202500258. https: //doi.org/10.1002/cmdc.202500258.

[29] Javaid, N.; Patra, M. C.; Cho, D.-E.; Batool, M.; Kim, Y.; Choi, G. M.; Kim, M. S.; Hahm, D.-H.; Choi, S. An Orally Active, Small-Molecule TNF Inhibitor That Disrupts the Homotrimerization Interface Improves Inflammatory Arthritis in Mice. Sci. Signal. 2022, 15 (759), eabi8713. https: //doi.org/10.1126/scisignal.abi8713.

[30] Schmidt, R. M. Recurrent Neural Networks (RNNs): A Gentle Introduction and Overview. arXiv 2019. https: //doi.org/10.48550/ARXIV.1912.05911.

[31] Vaswani, A.; Shazeer, N.; Parmar, N.; Uszkoreit, J.; Jones, L.; Gomez, A. N.; Kaiser, L.; Polosukhin, I. Attention Is All You Need. arXiv 2017. https: //doi.org/10.48550/ARXIV.1706.03762.

[32] Šali, A.; Blundell, T. L. Comparative Protein Modelling by Satisfaction of Spatial Restraints. Journal of Molecular Biology 1993, 234 (3), 779–815. https: //doi.org/10.1006/jmbi.1993.1626.

[33] Eberhardt, J.; Santos-Martins, D.; Tillack, A. F.; Forli, S. AutoDock Vina 1.2.0: New Docking Methods, Expanded Force Field, and Python Bindings. J. Chem. Inf. Model. 2021, 61 (8), 3891–3898. https: //doi.org/10.1021/acs.jcim.1c00203.

[34] Lu, D.; Luo, D.; Zhang, Y.; Wang, B. A Robust Induced Fit Docking Approach with the Combination of the Hybrid All-Atom/United-Atom/Coarse-Grained Model and Simulated Annealing. J. Chem. Theory Comput. 2024, 20 (14), 6414–6423. https: //doi.org/10.1021/acs.jctc.4c00653.

[35] Abraham, M. J.; Murtola, T.; Schulz, R.; Páll, S.; Smith, J. C.; Hess, B.; Lindahl, E. GROMACS: High Performance Molecular Simulations through Multi-Level Parallelism from Laptops to Supercomputers. SoftwareX 2015, 1–2, 19–25. https: //doi.org/10.1016/j.softx.2015.06.001.

DOI: 10.54254/2753-8818/2026.AU30170

[36] Abraham, M.; Alekseenko, A.; Basov, V.; Bergh, C.; Briand, E.; Brown, A.; Doijade, M.; Fiorin, G.; Fleischmann, S.; Gorelov, S.; Gouaillardet, G.; Gray, A.; Irrgang, M. E.; Jalalypour, F.; Jordan, J.; Kutzner, C.; Lemkul, J. A.; Lundborg, M.; Merz, P.; Miletic, V.; Morozov, D.; Nabet, J.; Pall, S.; Pasquadibisceglie, A.; Pellegrino, M.; Santuz, H.; Schulz, R.; Shugaeva, T.; Shvetsov, A.; Villa, A.; Wingbermuehle, S.; Hess, B.; Lindahl, E. GROMACS 2024.4 Source Code, 2024. https: //doi.org/10.5281/ZENODO.14016590.

[37] Showalter, S. A.; Brüschweiler, R. Validation of Molecular Dynamics Simulations of Biomolecules Using NMR Spin Relaxation as Benchmarks: Application to the AMBER99SB Force Field. J. Chem. Theory Comput. 2007, 3 (3), 961–975. https: //doi.org/10.1021/ct7000045.

[38] Sousa Da Silva, A. W.; Vranken, W. F. ACPYPE - AnteChamber PYthon Parser interfacE. BMC Res Notes 2012, 5 (1), 367. https: //doi.org/10.1186/1756-0500-5-367.

[39] Wang, J.; Wang, W.; Kollman, P. A.; Case, D. A. Automatic Atom Type and Bond Type Perception in Molecular Mechanical Calculations. Journal of Molecular Graphics and Modelling 2006, 25 (2), 247–260. https: //doi.org/10.1016/j.jmgm.2005.12.005.

[40] Wang, J.; Wolf, R. M.; Caldwell, J. W.; Kollman, P. A.; Case, D. A. Development and Testing of a General Amber Force Field. J Comput Chem 2004, 25 (9), 1157–1174. https: //doi.org/10.1002/jcc.20035.

[41] Mark, P.; Nilsson, L. Structure and Dynamics of the TIP3P, SPC, and SPC/E Water Models at 298 K. J. Phys. Chem. A 2001, 105 (43), 9954–9960. https: //doi.org/10.1021/jp003020w.

[42] Bussi, G.; Donadio, D.; Parrinello, M. Canonical Sampling through Velocity Rescaling. The Journal of Chemical Physics 2007, 126 (1), 014101. https: //doi.org/10.1063/1.2408420.

[43] Bernetti, M.; Bussi, G. Pressure Control Using Stochastic Cell Rescaling. The Journal of Chemical Physics 2020, 153 (11), 114107. https: //doi.org/10.1063/5.0020514.

[44] Van Gunsteren, W. F.; Berendsen, H. J. C. A Leap-Frog Algorithm for Stochastic Dynamics. Molecular Simulation 1988, 1 (3), 173–185. https: //doi.org/10.1080/08927028808080941.

[45] Luty, B. A.; Van Gunsteren, W. F. Calculating Electrostatic Interactions Using the Particle−Particle Particle−Mesh Method with Nonperiodic Long-Range Interactions. J. Phys. Chem. 1996, 100 (7), 2581–2587. https: //doi.org/10.1021/jp9518623.

[46] Michaud-Agrawal, N.; Denning, E. J.; Woolf, T. B.; Beckstein, O. MDAnalysis: A Toolkit for the Analysis of Molecular Dynamics Simulations. J Comput Chem 2011, 32 (10), 2319–2327. https: //doi.org/10.1002/jcc.21787.

[47] Meng, E. C.; Goddard, T. D.; Pettersen, E. F.; Couch, G. S.; Pearson, Z. J.; Morris, J. H.; Ferrin, T. E. UCSF ChimeraX: Tools for Structure Building and Analysis. Protein Science 2023, 32 (11), e4792. https: //doi.org/10.1002/pro.4792.

[48] Hunter, J. D. Matplotlib: A 2D Graphics Environment. Comput. Sci. Eng. 2007, 9 (3), 90–95. https: //doi.org/10.1109/MCSE.2007.55.

[49] Miller, B. R.; McGee, T. D.; Swails, J. M.; Homeyer, N.; Gohlke, H.; Roitberg, A. E. MMPBSA.Py: An Efficient Program for End-State Free Energy Calculations. J. Chem. Theory Comput. 2012, 8 (9), 3314–3321. https: //doi.org/10.1021/ct300418h.

[50] Valdés-Tresanco, M. S.; Valdés-Tresanco, M. E.; Valiente, P. A.; Moreno, E. gmx_MMPBSA: A New Tool to Perform End-State Free Energy Calculations with GROMACS. J. Chem. Theory Comput. 2021, 17 (10), 6281–6291. https: //doi.org/10.1021/acs.jctc.1c00645.

[51] Deringer, V. L.; Bartók, A. P.; Bernstein, N.; Wilkins, D. M.; Ceriotti, M.; Csányi, G. Gaussian Process Regression for Materials and Molecules. Chem. Rev. 2021, 121 (16), 10073–10141. https: //doi.org/10.1021/acs.chemrev.1c00022.

[52] Greg Landrum; Paolo Tosco; Brian Kelley; Ricardo Rodriguez; David Cosgrove; Riccardo Vianello; sriniker; Peter Gedeck; Gareth Jones; Eisuke Kawashima; NadineSchneider; Dan Nealschneider; Andrew Dalke; tadhurst-cdd; Matt Swain; Brian Cole; Samo Turk; Aleksandr Savelev; Alain Vaucher; Maciej Wójcikowski; Hussein Faara; Ichiru Take; Niels Maeder; Rachel Walker; Vincent F. Scalfani; Daniel Probst; Kazuya Ujihara; Axel Pahl; guillaume godin; Juuso Lehtivarjo. Rdkit/Rdkit: 2025_09_1 (Q3 2025) Release, 2025. https: //doi.org/10.5281/ZENODO.591637.

[53] Griffiths, R.-R.; Klarner, L.; Moss, H. B.; Ravuri, A.; Truong, S.; Stanton, S.; Tom, G.; Rankovic, B.; Du, Y.; Jamasb, A.; Deshwal, A.; Schwartz, J.; Tripp, A.; Kell, G.; Frieder, S.; Bourached, A.; Chan, A.; Moss, J.; Guo, C.; Durholt, J.; Chaurasia, S.; Strieth-Kalthoff, F.; Lee, A. A.; Cheng, B.; Aspuru-Guzik, A.; Schwaller, P.; Tang, J. GAUCHE: A Library for Gaussian Processes in Chemistry. arXiv 2022. https: //doi.org/10.48550/ARXIV.2212.04450.

[54] Frazier, P. I. A Tutorial on Bayesian Optimization. arXiv 2018. https: //doi.org/10.48550/ARXIV.1807.02811.

[55] Berk, J.; Gupta, S.; Rana, S.; Venkatesh, S. Randomised Gaussian Process Upper Confidence Bound for Bayesian Optimisation. arXiv 2020. https: //doi.org/10.48550/ARXIV.2006.04296.

DOI: 10.54254/2753-8818/2026.AU30170

[56] Balandat, M.; Karrer, B.; Jiang, D. R.; Daulton, S.; Letham, B.; Wilson, A. G.; Bakshy, E. BoTorch: A Framework for Efficient Monte-Carlo Bayesian Optimization. 2019. https: //doi.org/10.48550/ARXIV.1910.06403.
[57] Liang, S.; Dai, J.; Hou, S.; Su, L.; Zhang, D.; Guo, H.; Hu, S.; Wang, H.; Rao, Z.; Guo, Y.; Lou, Z. Structural Basis for Treating Tumor Necrosis Factor α (TNFα)-Associated Diseases with the Therapeutic Antibody Infliximab. Journal of Biological Chemistry 2013, 288 (19), 13799–13807. https: //doi.org/10.1074/jbc.M112.433961.
[58] Vugler, A.; O'Connell, J.; Nguyen, M. A.; Weitz, D.; Leeuw, T.; Hickford, E.; Verbitsky, A.; Ying, X.; Rehberg, M.; Carrington, B.; Merriman, M.; Moss, A.; Nicholas, J.-M.; Stanley, P.; Wright, S.; Bourne, T.; Foricher, Y.; Zhu, Z.; Brookings, D.; Horsley, H.; Heer, J.; Schio, L.; Herrmann, M.; Rao, S.; Kohlmann, M.; Florian, P. An Orally Available Small Molecule That Targets Soluble TNF to Deliver Anti-TNF Biologic-like Efficacy in Rheumatoid Arthritis. Front. Pharmacol. 2022, 13, 1037983. https: //doi.org/10.3389/fphar.2022.1037983.
[59] Chan, D. S.; Lee, H.; Yang, F.; Che, C.; Wong, C. C. L.; Abagyan, R.; Leung, C.; Ma, D. Structure-Based Discovery of Natural-Product-like TNF-α Inhibitors. Angew Chem Int Ed 2010, 49 (16), 2860–2864. https: //doi.org/10.1002/anie.200907360.
[60] Qiu, Z.; Huang, R.; Wu, Y.; Li, X.; Sun, C.; Ma, Y. Decoding the Structural Diversity: A New Horizon in Antimicrobial Prospecting and Mechanistic Investigation. Microbial Drug Resistance 2024, 30 (6), 254–272. https: //doi.org/10.1089/mdr.2023.0232.
[61] Xie, S.; Zhu, H.; Huang, N. AI-Designed Molecules in Drug Discovery, Structural Novelty Evaluation, and Implications. J. Chem. Inf. Model. 2025, 65 (17), 8924–8933. https: //doi.org/10.1021/acs.jcim.5c00921.
[62] König, G.; Miller, B. T.; Boresch, S.; Wu, X.; Brooks, B. R. Enhanced Sampling in Free Energy Calculations: Combining SGLD with the Bennett's Acceptance Ratio and Enveloping Distribution Sampling Methods. J. Chem. Theory Comput. 2012, 8 (10), 3650–3662. https: //doi.org/10.1021/ct300116r.
[63] York, D. M. Modern Alchemical Free Energy Methods for Drug Discovery Explained. ACS Phys. Chem Au 2023, 3 (6), 478–491. https: //doi.org/10.1021/acsphyschemau.3c00033.